Cp₂Mg-induced transition metal ion contamination and performance loss in MOCVD-grown blue emitting InGaN/GaN multiple quantum wells

Cite as: Appl. Phys. Lett. 116, 192106 (2020); doi: 10.1063/1.5142505 Submitted: 13 December 2019 · Accepted: 2 May 2020 · Published Online: 13 May 2020







Richard Liu, 1 📵 Eric Tucker, 2 📵 Soo Min Lee, 2 Kalyan Kasarla, 2 Callan McCormick, 1 📵 and Can Bayram 🗀 🗀





AFFILIATIONS

 1 Department of Electrical and Computer Engineering, University of Illinois at Urbana-Champaign, Illinois 61801, USA and Holonyak Micro and Nanotechnology Laboratory, University of Illinois at Urbana-Champaign, Illinois 61801, USA

ABSTRACT

The detrimental effects of Cp₂Mg-induced trace transition metal (iron and manganese) contamination on the optical performance of metalorganic chemical vapor deposition (MOCVD)-grown blue-emitting InGaN/GaN multiple quantum wells (MQWs) are investigated experimentally. Five samples are grown at various stages of conditioning of a freshly installed MOCVD tool with stainless steel gas lines. Without conditioning, Cp_2Mg flow induced Fe and Mn impurities with concentrations of 3×10^{15} and 3×10^{14} cm⁻³, respectively. These contaminants introduce nonradiative recombination centers with lifetimes on the order of nanoseconds. These impurities also induce indium-clustering related phenomena such as low energy shoulder at low temperature and a strong S-curve shift in emission energy with increasing temperature. Through successive cycles of chamber conditioning, the Fe and Mn concentrations decrease to below their detection limits, and the nonradiative recombination lifetime (+8 ns), internal quantum efficiency (+26%), microphotoluminescence nonuniformity (-4.7%), and S-curve shift (-26 meV) of the MQWs improved. The suppression of the transition metal ion contamination in the MOCVD chamber is shown to be crucial for high performance MQWs and blue light emitting diode growths.

Published under license by AIP Publishing. https://doi.org/10.1063/1.5142505

Group III-nitride semiconductors have transformed the solid state lighting industry through the commercialization of blue-emitting InGaN/GaN multiple quantum wells (MQWs) and their phosphorcoated variant white-emitting light emitting diodes (LEDs) that have high efficiency, long service life, high brightness, and small footprint.1 These devices are most often commercially grown on Al₂O₃ or SiC substrates using metal organic chemical vapor deposition (MOCVD) due to its high throughput. Typically, the main layers in the LED epi wafer consist of a p-i-n structure with n-type GaN as the bottom layer, the InGaN/GaN MQW in the intrinsic region, and Mg-doped p-type GaN as the top layer.

The conventional precursor for Mg-doping in the p-type GaN layer is bis(cyclopentadienyl)magnesium (Cp2Mg).2 Since Mg is the strongest reductant ($E_{Me^{2+}}^0 = -2.382 \,\text{eV}$) of the metal species found

in a stainless steel MOCVD reactor, it is capable of reducing Cr₂O₃, which is the self-healing passivation layer that forms on typical 316 stainless steel to prevent oxidation of other transition metal constituents, such as Fe and Mn.³ Therefore, introducing Cp₂Mg in a pristine MOCVD chamber for the first time could induce this transmetalation to form MgO, which itself limits further reaction once the lining is covered with it. Cr ($E^0_{Cr^{3+}}=-0.74$ eV), along with the underlying Fe ($E^0_{Fe^{3+}}=-0.04$ eV) and Mn ($E^0_{Cr^{3+}}=-0.74$ eV) ions that are now present on the lining of the gas lines, can be entrained in the gas flow (TMAl, TMGa, and TMIn) of the next epitaxial run and transported inadvertently to the growth surface.^{4,5} These metallic ion impurities then act as traps with large capture cross sections in GaN (Fe_{Ga}: $2.1-2.5 \,\mathrm{eV}^6$ and Mn_{Ga} : $1.4 \,\mathrm{eV}^7$ above the valence band) to create efficient nonradiative recombination centers that reduce the devices'

²Veeco Instruments, Inc., Somerset, New Jersey 08873, USA

^{a)}Present address: Innovative COmpound semiconductoR (ICORLAB), Urbana, Illinois, USA.

^{b)}Author to whom correspondence should be addressed: cbayram@illinois.edu. URL: https://www.icorlab.ece.illinois.edu. Tel.: +1(217) 300-0978. Fax: +1(217) 244-6375

efficiency. 8-12 Suppressing the entrainment of these impurities usually takes numerous epitaxial growths to thoroughly season the MOCVD chamber since first principles studies have shown that iron concentrations as low as 10¹⁵ cm⁻³ can have a significant negative impact on the device performance due to the large carrier capture cross section of its excited states. 12 This paper examines this effect experimentally in a typical conditioning procedure carried out in a commercial MOCVD chamber using optical and structural characterization techniques.

In this paper, five samples (MQW1–5) each consisting of six pairs of In_{0.15}Ga_{0.85}N/GaN quantum well barriers on a 5- μ m thick GaN buffer layer on 6-in. Al₂O₃ substrates are grown during various stages of the conditioning of a never-used MOCVD chamber. Each cycle of conditioning (Mg-conditioning) is composed of (i) high flux Cp₂Mg flow to initiate the transmetalation followed by (ii) opening the chamber for ambient air and humidity exposure to fully oxidize Mg.¹³ MQW1 is grown after the initial cycle high flux Cp₂Mg. MQW2 is grown after five additional cycles of Mg-conditioning. MQW3 is grown after one additional cycle. MQW4 is grown after multiple additional cycles. MQW5 is grown after yet more additional cycles.

Structural characterization techniques, such as atomic force microscopy, x-ray diffraction, and reciprocal space mapping, are conducted on the samples, and no observable differences are found among the samples (see the supplementary material, Figs. S1–S4). Secondary ion mass spectroscopy is conducted on a Cameca IMS with O_2 plasma to measure the trace concentration of Fe and Mn impurities. MQW1 is found to contain approximately $3 \times 10^{14} \, \mathrm{cm}^{-3}$ of Mn and $3 \times 10^{15} \, \mathrm{cm}^{-3}$ of Fe. No other samples were found to contain more than $1 \times 10^{14} \, \mathrm{cm}^{-3}$ of Mn and $1 \times 10^{15} \, \mathrm{cm}^{-3}$ of Fe, which are the detection limits of the instrument (Figs. S5 and S6). A similar level ($10^{15} \, \mathrm{cm}^{-3}$) of unintentional Fe contamination has been reported in hydride vapor phase epitaxy (HVPE) growth of GaN when a Mg dopant is used. Using electron paramagnetic resonance (EPR), signals from Fe impurities are observed; this corroborates the observation from the SIMS data.

The optical properties of the MQW samples are measured using room temperature photoluminescence (PL) with a $\lambda = 266 \, \text{nm}$ laser and spectrometer fitted with a CCD camera (Fig. 1). All five samples show their peak emission energy at roughly 2.77 eV (448 nm). Overall, the PL intensity increases with successive cycles of Mg-conditioning with MQW1 (no conditioning) showing the lowest intensity and MQW5 (most extensive conditioning and air exposure) showing the highest. The samples show a maximum integrated PL intensity increase of 41% and peak intensity by 52% (MQW5). No defectrelated luminescence (e.g., the yellow luminescence band) is observed. The effectiveness of chamber conditioning at increasing the PL intensity is significant; growing MQW structures in an unconditioned stainless steel chamber after initial Cp2Mg exposure introduces Fe and Mn impurities that reduce the PL intensity. With multiple cycles of Mg-conditioning and MQW growth, the contamination mechanism is suppressed, and the PL intensity gradually recovers to the same intensity as the sample grown before Cp2Mg was introduced in the chamber (Fig. S7).

Additional to the overall PL intensity, spatial and spectral emission uniformity is examined using a micro-PL (μ PL) setup with a $\lambda=325\,\mathrm{nm}$ continuous wave laser. Figure 2 shows the integrated PL intensity mapping of the samples relative to their respective averages in a $200\times200\,\mu\mathrm{m}^2$ area. The intensity distribution in MQW1, which

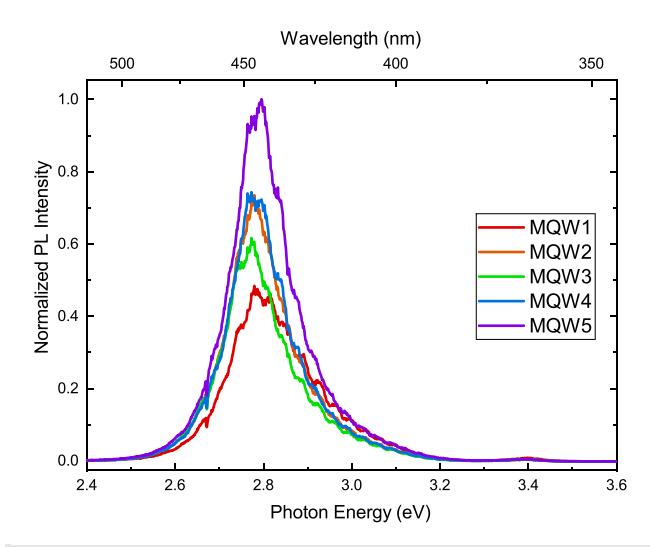


FIG. 1. PL spectra of the MQW samples, which show PL peaks at 2.77 eV ($\lambda=448\,\mathrm{nm}$). The sample with the most Fe and Mn impurities (MQW1) shows the weakest integrated PL intensity. Multiple cycles of chamber conditioning increase the PL intensity.

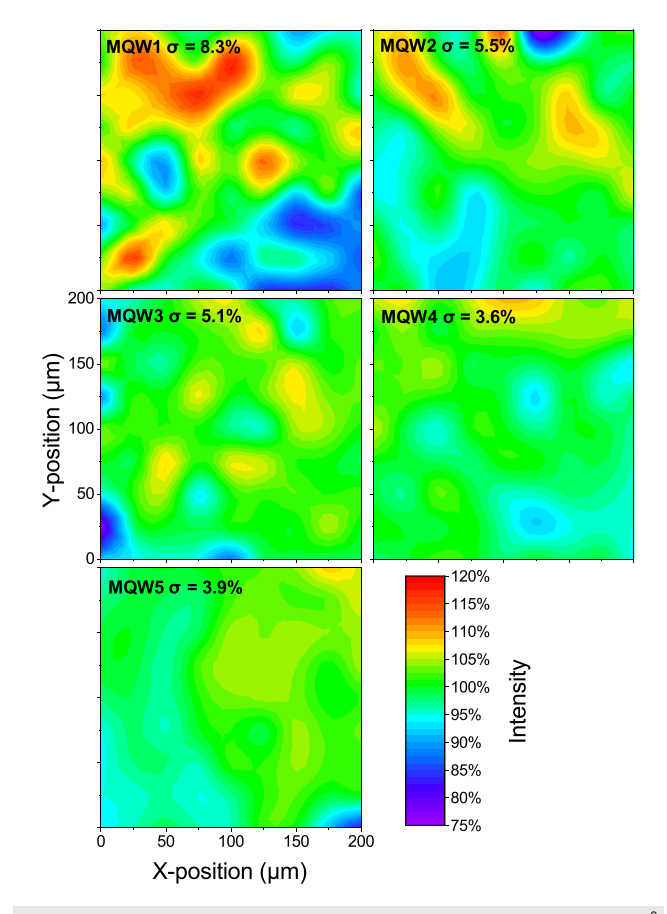


FIG. 2. Micro-PL mapping of the intensities of the samples over a $200 \times 200 \ \mu\text{m}^2$ area. Each figure is scaled relative to its own average. The standard deviations are also shown.

has the most of Fe and Mn impurities and lowest PL intensity, shows the highest level of nonuniformity (σ) of 8.3% (Fig. 2). This sample shows numerous dark spots as dim as 17% weaker than its average. With the five and six cycles of Mg-conditioning, MQW2 and MQW3 show reduced σ values of 5.5 and 5.1%, respectively. The trend continues with MQW4 and MQW5, which show σ values of 3.6% and 3.9%, respectively. These data suggest that the Fe and Mn impurities maybe the culprit in creating localized nonradiative recombination centers, which reduces the overall PL intensity.

To study the optical properties of the samples in the temporal space, time-resolved PL (TRPL) is conducted (Fig. 3) using a frequency-doubled, femtosecond Ti:sapphire laser ($\lambda = 385$ nm, 1 nJ pulses) and an avalanche photodiode with bandpass filters for data collection. MQW1 shows biexponential decay PL lifetimes (τ_{PI}) of 0.8 and 2.78 ns at a time interval between $0 \sim 2$ ns and $2 \sim 6$ ns after laser pulse incidence, respectively, while MQW2 and MQW3 show a similar monoexponential τ_{PL} of \sim 3.79 ns, and MQW4 and MQW5 show an additional increase in τ_{PL} to \sim 4.43 ns. This suggests that the initial cycles of the Mg-condition (MQW2) reduced a vast majority of the nonradiative recombination centers, likely caused by the Fe and Mn impurities, which are responsible for the difference in τ_{PL} . A few additional cycles (MQW3 and MQW4) and further cycles of Mg/air exposures (MQW5) yielded only small increases in over MQW2. This demonstrates the importance of eliminating these transition metal contaminants even at very low concentrations.

To study the effect of these nonradiative recombination centers in MQW1 and their reduction in the other samples, temperature-dependent (6–300 K) PL is conducted using a $\lambda=266$ nm laser and a liquid helium bath cryostat with a proportional integral differential (PID) temperature controller (Fig. 4). The temperature-dependent internal quantum efficiency (IQE) is calculated using

$$IQE(T) = \frac{I(T)}{I(6 \text{ K})},\tag{1}$$

where I(T) is the integrated intensity of the PL emission at temperature T, assuming that at 6 K, the recombination mechanism is purely

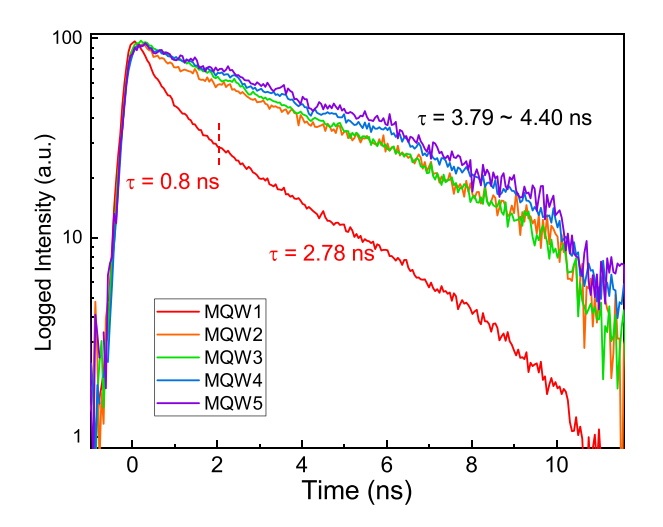


FIG. 3. Time-resolved PL using a 385 nm laser shows that MQW1 exhibits a biexponential decay, whereas the remaining samples have monoexponential decays with much longer lifetimes.

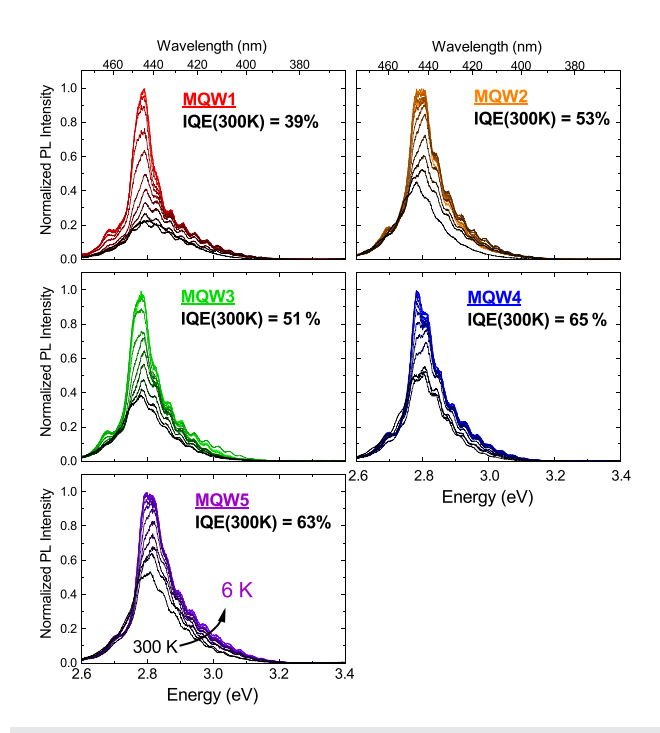


FIG. 4. Temperature-dependent PL spectra of the samples from $6\,\mathrm{K}$ to $300\,\mathrm{K}$. MQW1 has the lowest IQE (39% at room temperature) of all devices. Mg-conditioning improves the IQE from 39% to a maximum of 65%.

radiative. ¹⁵ MQW1 exhibits the lowest IQE of 39% at 300 K, whereas MQW2 and MQW3 exhibit similar IQEs at 53 and 51%, respectively. This suggests that the chamber conditioning eliminates a significant number of the nonradiative recombination centers and increases the IQE. Multiple additional cycles of Mg-conditioning have a diminishing return (MQW4 and MQW5) with IQEs that show an additional 10% increase (IQE > 60%). The observation made on the trend of IQE across the samples roughly mirrors that of the integrated PL intensities (Fig. 1) and TRPL (Fig. 3); chamber conditioning decreases the rate of nonradiative recombination. Similarities in the trend between these three characterization techniques suggest that the differences in observed optical properties originate from the same nonradiative recombination centers introduced by the Fe and Mn impurities that reduce PL intensity, shorten PL lifetime, and reduce IQE.

Closer inspection of the temperature-dependent PL spectra revealed that all samples exhibit a low energy PL peak at 2.7 eV at temperatures below 100 K. This emission center has been associated with potential minima caused by local indium clustering 16 and is especially prominent in MQW1 and becomes less prominent with successive Mg-conditioning. Studies have shown that some impurities (e.g., Si) in the InGaN/GaN MQW on Al $_2$ O $_3$ can result in the formation of nanoscale high indium content clusters. 17,18 The data here suggest that this phenomenon may also occur with Fe or Mn impurities.

The extracted PL peak emission energy and peak emission energy shift from their 6 K values as a function of temperature, which are plotted in Fig. 5. All five samples show a distinct blueshift in the peak emission energy as the temperature decreases from 300 K; the trend then reverses to red-shifting at temperatures below 170 K, and finally,

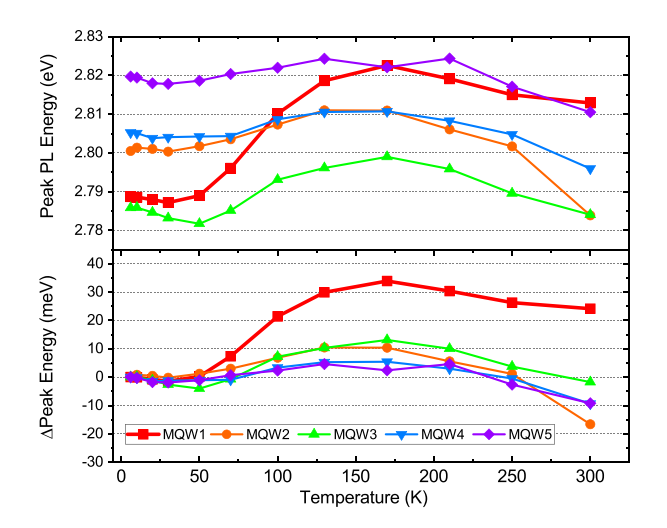


FIG. 5. (Top) Temperature dependent peak PL emission energies. (Bottom) Peak emission energy shift from its 6 K value.

the trend reverses again to blue-shifting at temperatures below 20 K. This s-shaped redshift-blueshift-redshift behavior is attributed to the carrier localization in the inhomogeneity in the InGaN MQWs. Comparing the magnitudes of the blueshift at 170 K, MQW1 shows an exceptionally strong shift at 36 meV. While MQW2 and MQW3 only blue shift by $\sim\!10$ meV, MQW4 and MQW5 blue shift by an even smaller amount at $\sim\!5$ meV. At temperatures higher than 170 K, all samples red shift at a similar rate. This progressive reduction in the magnitude of the S-curve in the samples with increasing cycles of conditioning shows a correlation between Fe and Mn impurities and the carrier dynamics in the quantum wells; these atoms induce inhomogeneity in the InGaN layer. This phenomenon does not appear to be significant when the impurity concentrations fall below the detection limit

This relationship is consistent with the observations made in the μ PL uniformity measurements showing a decrease in integrated PL nonuniformity from MQW1 to MQW5 and mirrors the decrease in the intensity of the 2.7 eV low energy shoulder in low temperature PL results from MQW1 to MQW5, in which the strongest effect is found in the sample with Fe and Mn impurity concentrations above 10^{15} cm⁻³ and 10^{14} cm⁻³, respectively.

The IQE values can be used in conjunction with the carrier lifetime obtained from TRPL to calculate the radiative and nonradiative recombination lifetimes using¹⁵

$$IQE = \frac{\tau_{rad}^{-1}}{\tau_{PL}^{-1}},\tag{2}$$

where τ_{rad} and τ_{PL} are the radiative and PL lifetimes, which allows the extraction of nonradiative recombination lifetimes (τ_{nr}) via

$$\tau_{PL}^{-1} = \tau_{rad}^{-1} + \tau_{nr}^{-1}.\tag{3}$$

The extracted lifetimes of the samples are shown in Fig. 6.

The radiative lifetimes of the samples are calculated to be in the neighborhood of 7 ns. This is expected as the physical structures [quantum well (QW) layer thicknesses], strain, defectivity, and

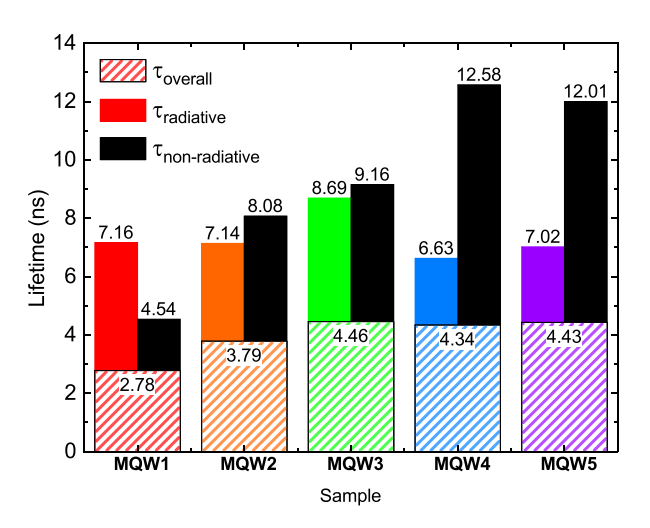


FIG. 6. Radiative and nonradiative lifetimes calculated using the TRPL and IQE measurements.

composition are statistically the same, and the values fall within the reported range for InGaN-based blue emitting MQWs. 20 The variation in τ_{nr} shows the detrimental effect of Fe and Mn impurities; MQW1 exhibits a very fast τ_{nr} (4.54 ns). Reducing their concentrations in MQW2 increases τ_{nr} by a significant 3.54 ns. At the low injection level presented here, nonradiative recombination can be assumed to be dominated by Shockley–Reed–Hall recombination (SRH), the A coefficient, which can be expressed as 21

$$A = \frac{1}{\tau_{nr}}. (4)$$

The increase in τ_{nr} between MQW1 and MQW2 corresponds to a decrease in the SRH coefficient from $2.2 \times 10^8 \, \rm s^{-1}$ to $1.2 \times 10^8 \, \rm s^{-1}$. The $1 \times 10^8 \, \rm s^{-1}$ reduction in the SRH recombination rate, coinciding with the reduction in the Fe impurity concentration from $3 \times 10^{15} \, \rm cm^{-3}$ to below the detection limit, is in good agreement with the rate reported in the literature. 12,22

One additional cycle of Mg-conditioning increases τ_{nr} by another ~ 1 ns in MQW3. This suggests that the chamber conditioning is not yet complete even with the impurity concentrations below the detection limit. Additional extensive Mg-conditioning before MQW4 was grown increased its τ_{nr} by another ~ 3 ns, but further cycles did not yield a significant improvement in MQW5. These suggest that the benefit of chamber conditioning has a diminishing return with the majority of the contaminants suppressed within the first five cycles of Mg-conditioning.

Conditioning of the MOCVD chamber appears to be complete somewhere between MQW3 and MQW4 using characterization techniques such as μ PL, IQE, and TRPL, which show no significant difference between MQW4 and MQW5. As far as these techniques show, the origin of the loss in optical performance seems to be fully suppressed after \sim 10+ cycles of Mg-conditioning. The largest performance gained was during the first five cycles that also coincide with the reduction in Fe and Mn impurity concentrations. The data suggest that these transition metal impurities affect the optical performance of blue-emitting InGaN/GaN MQWs at a concentration slightly below the SIMS detection limit of 10^{15} cm $^{-3}$.

In conclusion, through temperature-dependent, time-resolved, and μ PL, the detrimental effects of Fe and Mn impurities in blue-emitting InGaN/GaN MQWs are quantified. Even at very low concentrations (3 × 10¹⁵ and 3 × 10¹⁴ cm⁻³, respectively), these impurities are capable of forming efficient nonradiative recombination centers with recombination rates in the 10^8 s⁻¹ range. Through successive conditioning of the chamber, the impurities were reduced to below the detection limit, and IQE increased by 26%, μ PL intensity variation decreased by 4.7%, nonradiative recombination lifetime increased by 8 ns, and the magnitude of the S-curve shift decreased by 86%. Unintentional trace transition metal ion impurity contamination has been shown experimentally to play a significant role in the conditioning of MOCVD chambers.

See the supplementary material for the complete structural characterization using the atomic force microscopy defectivity study, x-ray diffraction, reciprocal space mapping, and secondary ion mass spectroscopy of the samples.

This work was supported by the National Science Foundation (NSF) Faculty Early Career Development (CAREER) Program under Award No. NSF-ECCS-16-52871. R. Liu acknowledges the support from the NASA Space Technology Research Fellowship (No. NSTRF-17). C. McCormick acknowledges the support from the National Science Foundation Faculty Early Career Development (CAREER) Program under Award No. NSF ECCS 16-52871 CAR REU. This study was carried out at the Nick Holonyak, Jr., Micro and Nanotechnology Laboratory, and Frederick Seitz Materials Research Laboratory Central Research Facilities, University of Illinois at Urbana-Champaign, IL, USA. The authors acknowledge the support from Dr. Tim Spila and Dr. Julio Suarez from the University of Illinois at Urbana-Champaign, IL, USA, for the secondary ion mass spectrometry and photoluminescence and Dr. Frank Ramos of Veeco for reviewing and advising on SIMs and other trace metal analysis results.

DATA AVAILABILITY

The data that support the findings of this study are available from the corresponding author upon reasonable request.

REFERENCES

- ¹S. Nakamura and M. R. Krames, "History of gallium-nitride-based light-emitting diodes for illumination," Proc. IEEE 101, 2211–2220 (2013).
- ²H. Amano, M. Kito, K. Hiramatsu, and I. Akasaki, "P-type conduction in mg-doped gan treated with low-energy electron beam irradiation (LEEBI)," Jpn. J. Appl. Phys., Part 2 28, L2112–L2114 (1989).
- 3A. Kimura, M. Shibata, K. Kondoh, Y. Takeda, M. Katayama, T. Kanie, and H. Takada, "Reduction mechanism of surface oxide in aluminum alloy powders containing magnesium studied by x-ray photoelectron spectroscopy using synchrotron radiation," Appl. Phys. Lett. 70, 3615–3617 (1997).
- ⁴B. Monemar and O. Lagerstedt, "Properties of VPE-grown GaN doped with Al and some iron-group metals," J. Appl. Phys. **50**, 6480–6491 (1979).

- ⁵G. Milazzo, S. Caroli, and R. D. Braun, "Tables of standard electrode potentials," J. Electrochem. Soc. 125, 261C (1978).
- ⁶K. Pressel, S. Nilsson, R. Heitz, A. Hoffmann, and B. K. Meyer, "Photoluminescence study of the 1.047 eV emission in GaN," J. Appl. Phys. 79, 3214–3218 (1996).
- ⁷R. Y. Korotkov, J. M. Gregie, and B. W. Wessels, "Optical properties of the deep Mn acceptor in GaN:Mn," Appl. Phys. Lett. 80, 1731–1733 (2002).
- ⁸C. Y. Hwang, M. J. Schurman, W. E. Mayo, Y. C. Lu, R. A. Stall, and T. Salagaj, "Effect of structural defects and chemical impurities on hall mobilities in low pressure MOCVD grown GaN," J. Electron. Mater. 26, 243–251 (1997)
- pressure MOCVD grown GaN," J. Electron. Mater. 26, 243–251 (1997).

 S. Leone, F. Benkhelifa, L. Kirste, C. Manz, S. Mueller, R. Quay, and T. Stadelmann, "Suppression of Iron Memory Effect in GaN Epitaxial Layers," Phys. Status Solidi B 255, 1700377–1700377 (2018).
- ¹⁰C. Liu, E. Alves, A. D. Sequeira, N. Franco, M. F. da Silva, and J. C. Soares, "Fe ion implantation in GaN: Damage, annealing, and lattice site location," J. Appl. Phys. 90, 81–86 (2001).
- ¹¹A. Y. Polyakov, N. B. Smirnov, A. V. Govorkov, N. V. Pashkova, A. A. Shlensky, S. J. Pearton, M. E. Overberg, C. R. Abernathy, J. M. Zavada, and R. G. Wilson, "Electrical and optical properties of Cr and Fe implanted n-GaN," J. Appl. Phys. 93, 5388–5396 (2003).
- ¹²D. Wickramaratne, J.-X. Shen, C. E. Dreyer, M. Engel, M. Marsman, G. Kresse, S. Marcinkevičius, A. Alkauskas, and C. G. Van de Walle, "Iron as a source of efficient Shockley-Read-Hall recombination in GaN," Appl. Phys. Lett. 109, 162107 (2016).
- ¹³C. Fotea, J. Callaway, and M. R. Alexander, "Characterisation of the surface chemistry of magnesium exposed to the ambient atmosphere," Surf. Interface Anal. 38, 1363–1371 (2006).
- ¹⁴M. E. Zvanut, J. Dashdorj, J. A. Freitas, E. R. Glaser, W. R. Willoughby, J. H. Leach, and K. Udwary, "Incorporation of Mg in free-standing HVPE GaN substrates," J. Electron. Mater. 45, 2692–2696 (2016).
- ¹⁵Y. Narukawa, Y. Kawakami, S. Fujita, and S. Nakamura, "Dimensionality of excitons in laser-diode structures composed of InGaN multiple quantum wells," Phys. Rev. B 59, 10283–10288 (1999).
- ¹⁶Y.-S. Lin, K.-J. Ma, C. Hsu, S.-W. Feng, Y.-C. Cheng, C.-C. Liao, C. C. Yang, C.-C. Chou, C.-M. Lee, and J.-I. Chyi, "Dependence of composition fluctuation on indium content in InGaN/GaN multiple quantum wells," Appl. Phys. Lett. 77, 2988–2990 (2000).
- 17Y. C. Cheng, S. W. Feng, E. C. Lin, C. C. Yang, C. H. Tseng, H. Cheng, and K. J. Ma, "Quantum dot formation in InGaN/GaN quantum well structures with silicon doping and the mechanisms for radiative efficiency improvement," Phys. Status Solidi C 0, 1093–1096 (2003).
- ¹⁸Y. C. Cheng, E. C. Lin, C. M. Wu, C. C. Yang, J. R. Yang, A. Rosenauer, K. J. Ma, S. C. Shi, L. C. Chen, C. C. Pan, and J. I. Chyi, "Nanostructures and carrier localization behaviors of green-luminescence InGaN/GaN quantum-well structures of various silicon-doping conditions," Appl. Phys. Lett. 84, 2506–2508 (2004).
- ¹⁹Y.-H. Cho, G. H. Gainer, A. J. Fischer, J. J. Song, S. Keller, U. K. Mishra, and S. P. DenBaars, "'S-shaped' temperature-dependent emission shift and carrier dynamics in InGaN/GaN multiple quantum wells," Appl. Phys. Lett. 73, 1370–1372 (1998).
- ²⁰C. Du, X. Huang, C. Jiang, X. Pu, Z. Zhao, L. Jing, W. Hu, and Z. L. Wang, "Tuning carrier lifetime in InGaN/GaN LEDs via strain compensation for high-speed visible light communication," Sci. Rep. 6, 37132 (2016).
- ²¹J. F. Muth, J. H. Lee, I. K. Shmagin, R. M. Kolbas, H. C. Casey, B. P. Keller, U. K. Mishra, and S. P. DenBaars, "Absorption coefficient, energy gap, exciton binding energy, and recombination lifetime of GaN obtained from transmission measurements," Appl. Phys. Lett. 71, 2572–2574 (1997).
- ²²D. Wickramaratne, J. X. Shen, C. E. Dreyer, A. Alkauskas, and C. G. Van De Walle, "Electrical and optical properties of iron in GaN, AlN, and InN," Phys. Rev. B 99, 205202 (2019).

Supplementary Material for:

"Cp₂Mg-Induced Transition Metal Ion Contamination and Performance Loss in MOCVD-Grown Blue Emitting InGaN/GaN Multiple Quantum Wells"

Richard Liu,¹ Eric Tucker,² Soo Min Lee,² Kalyan Kasarla,² Callan McCormick,¹ Can Bayram^{*1}

Nick Holonyak, Jr. Micro and Nanotechnology Laboratory, University of Illinois at Urbana-Champaign, Illinois, 61801, USA

This document contains the following:

Figure S1

Figure S2

Figure S3

Figure S4

Figure S5

Figure S6

Figure S7

¹Department of Electrical and Computer Engineering, University of Illinois at Urbana-Champaign, Illinois, 61801, USA

²Veeco Instruments, Inc, Somerset, New Jersey, 08873, USA

^{*} email: cbayram@illinois.edu, website: https://icorlab.ece.illinois.edu; phone: +1(217) 300-0978; fax: +1(217) 244-6375

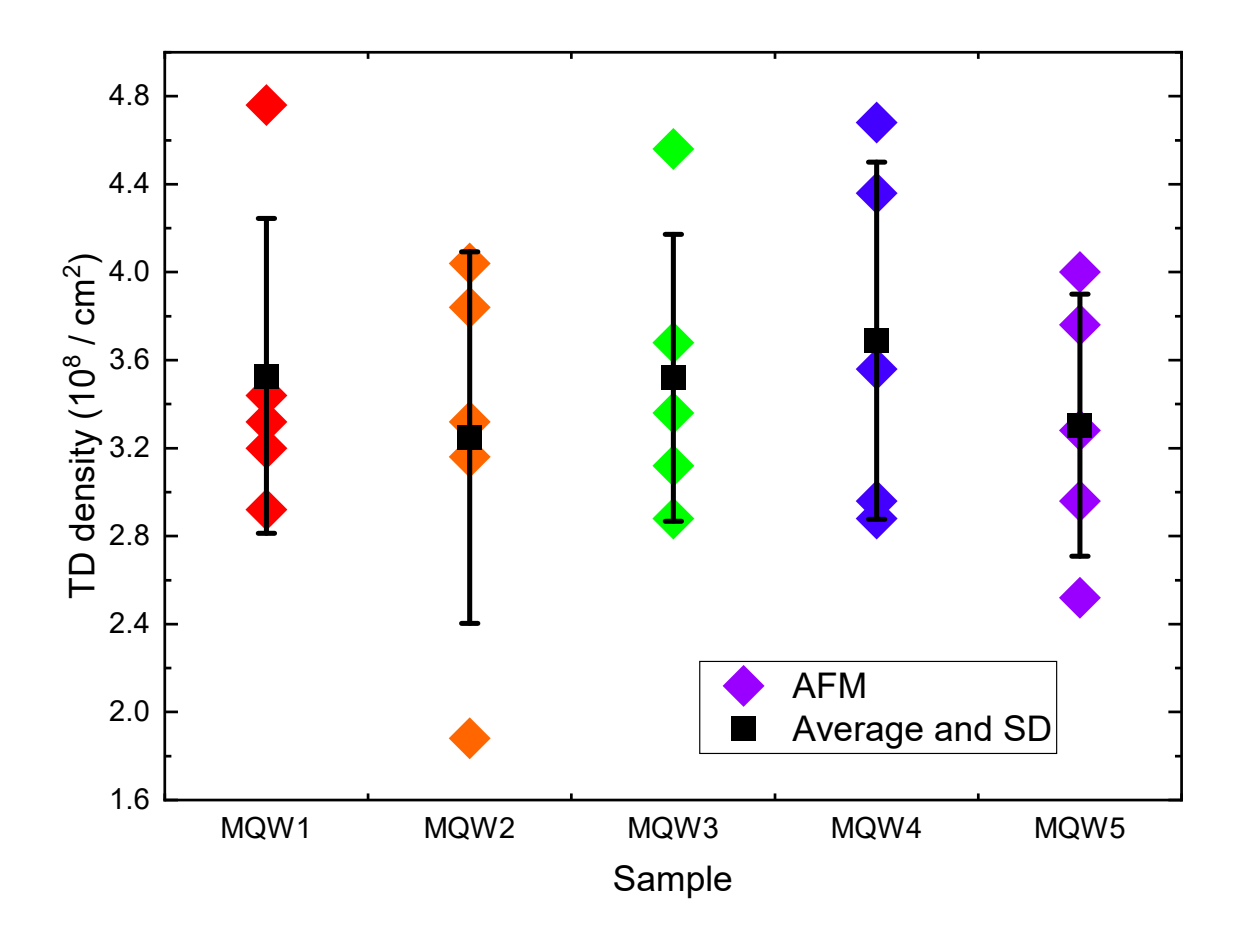


Figure S 1 Atomic force microscopy surface defectivity of the samples. The data is shown in color, and the average (standard deviation) is shown in black squares (black lines)

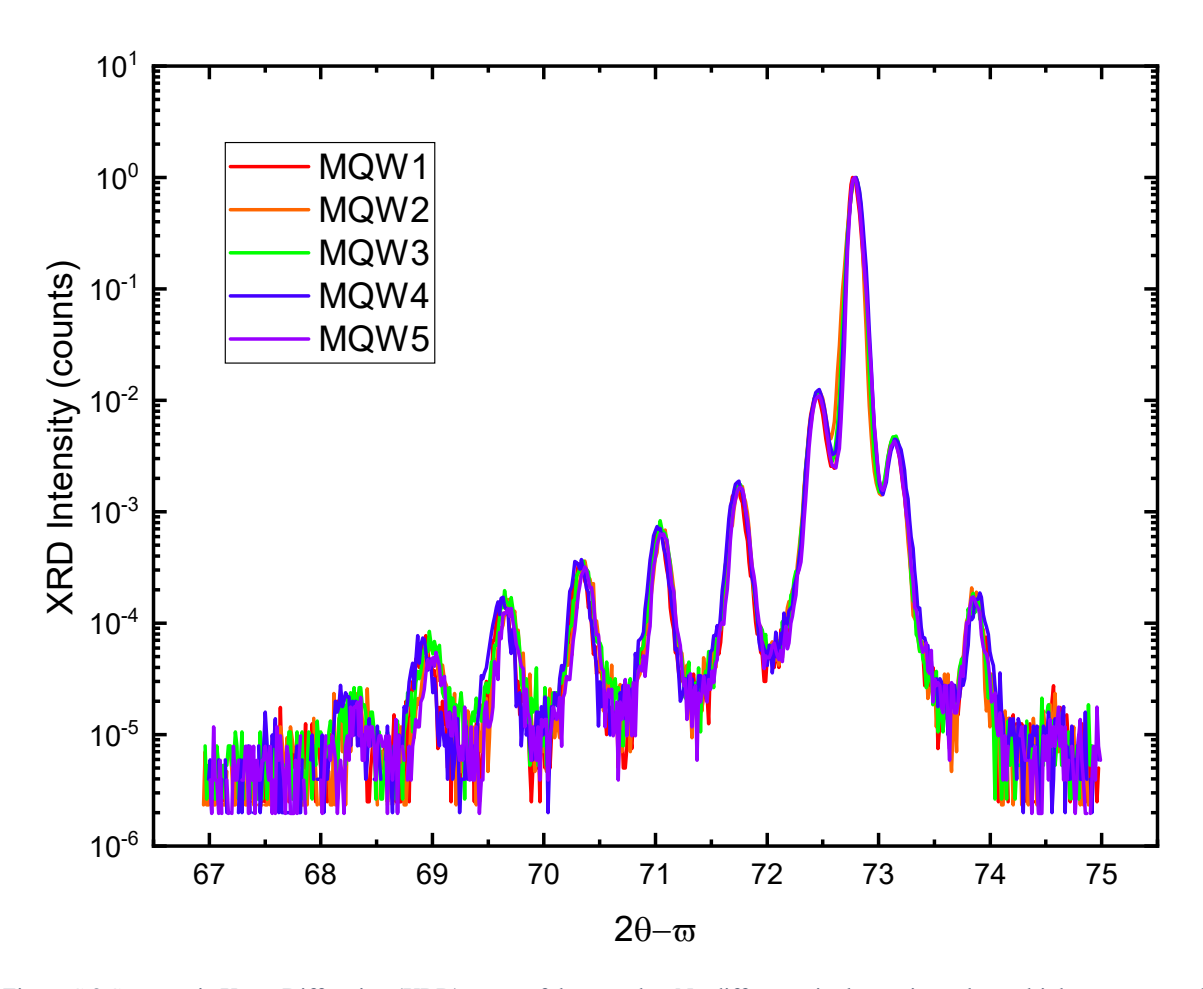


Figure S 2 Symmetric X-ray Diffraction (XRD) scans of the samples. No difference in the strain or the multiple quantum well composition and dimensions are observed.

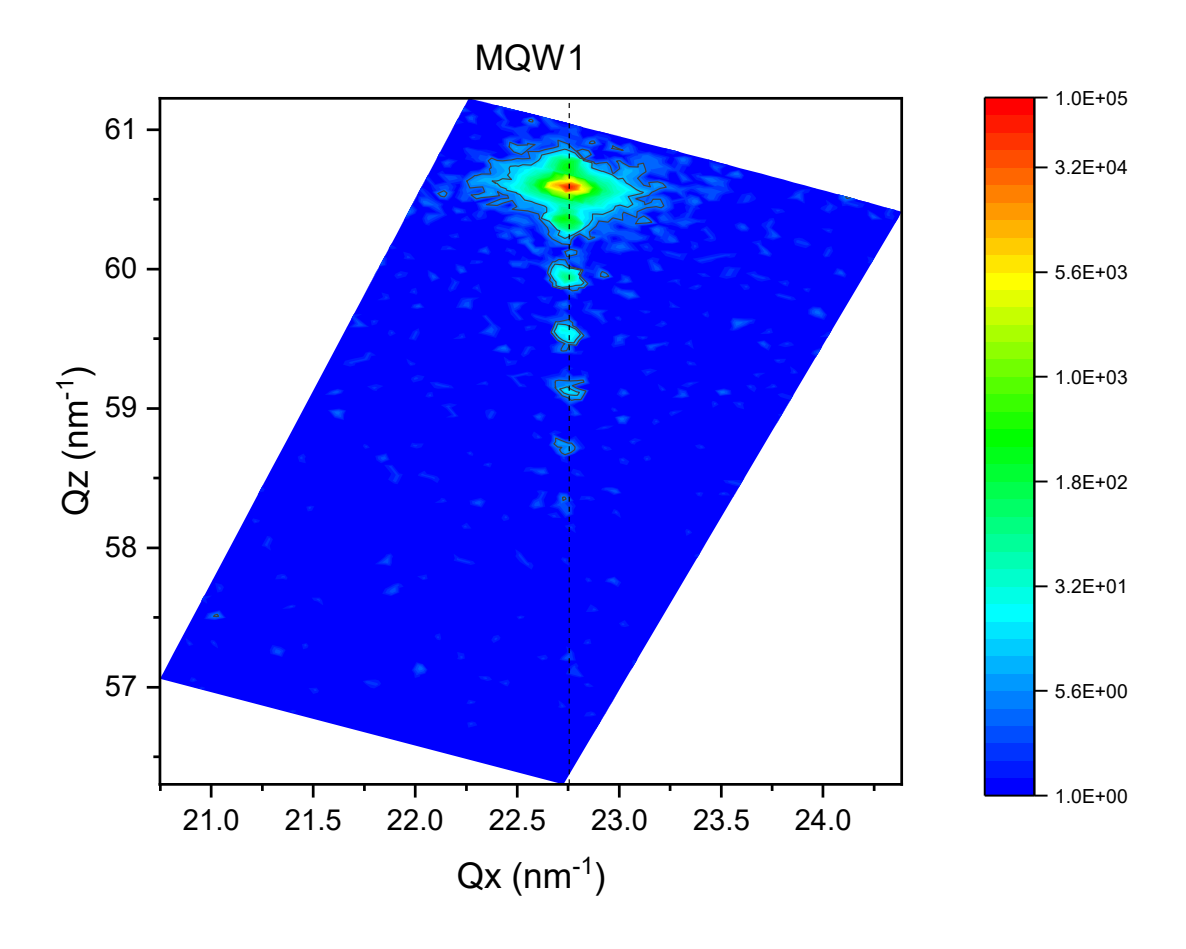


Figure S 3 Reciprocal space mapping (RSM) of sample MQW1. The vertical dashed line shows that the InGaN MQWs are fully strained

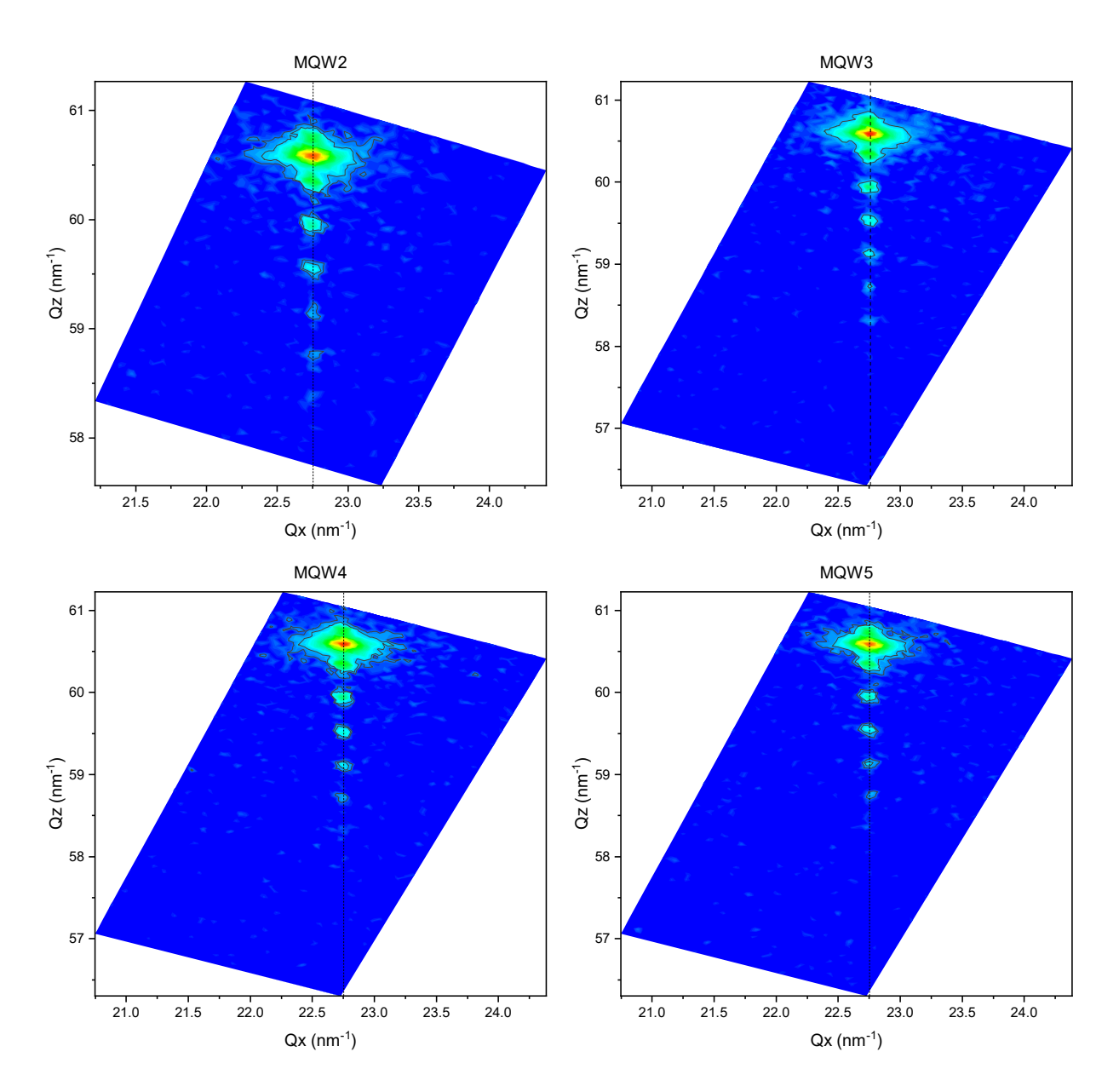


Figure S 4 RSM of samples MQW2 to MQW5. All samples show full strained InGaN MQWs.

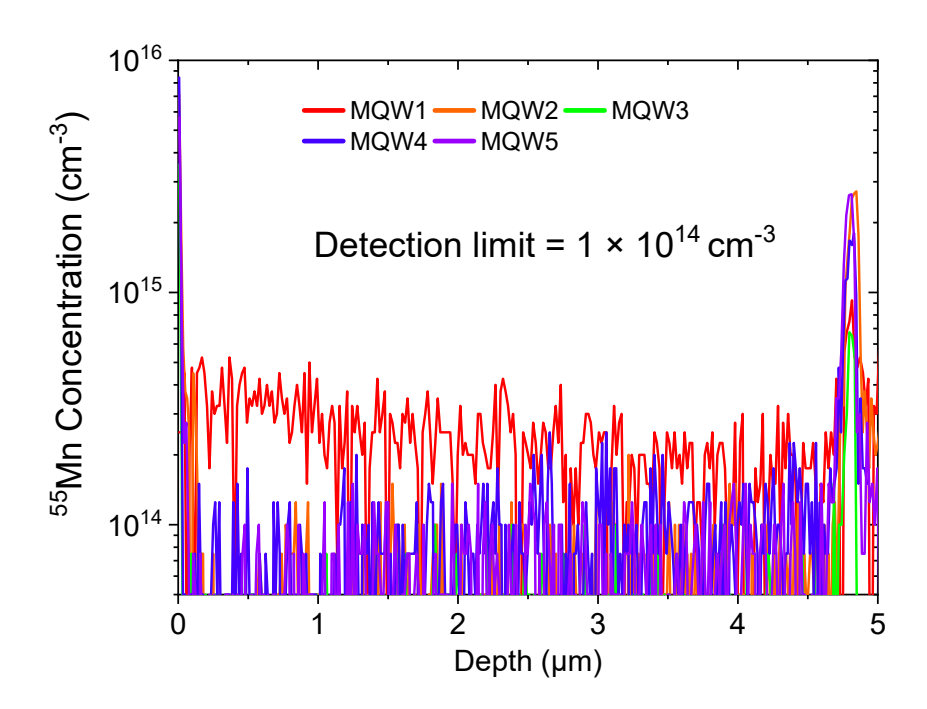


Figure S 5 SIMS data for ⁵⁵Mn

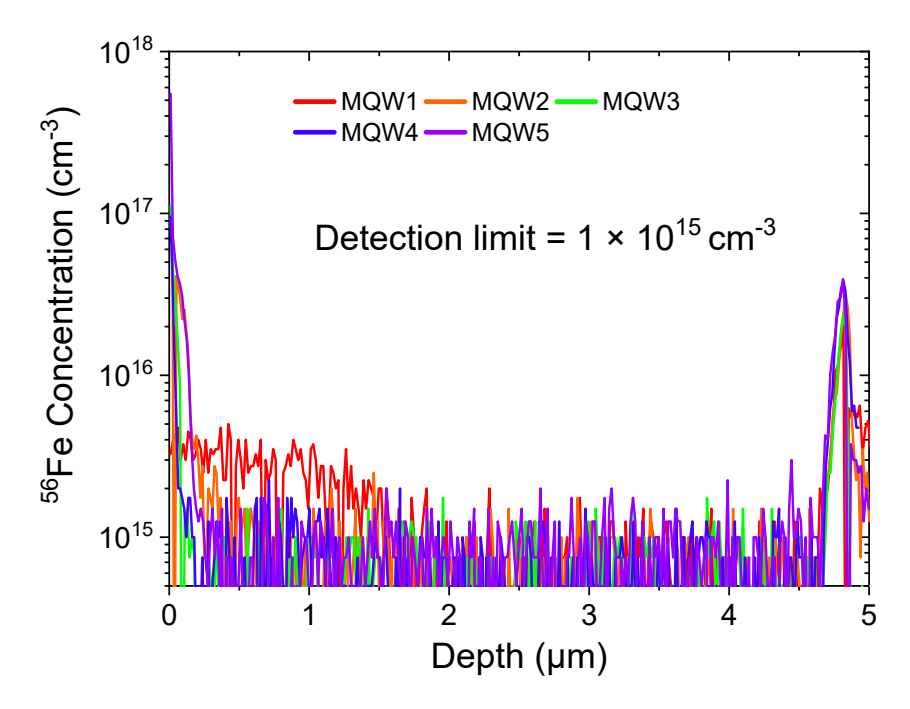


Figure S 6 SIMS data for ⁵⁶Fe

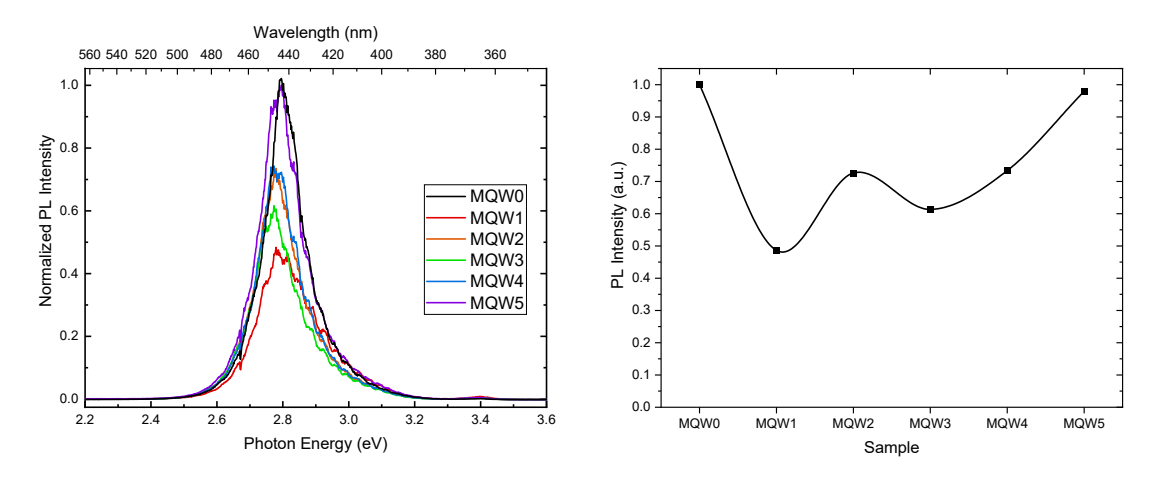


Figure S 7 (left) PL spectra of the MQW samples with MQW0 (sample grown before any Mg was introduced to the chamber) included which all show PL peaks at 2.77 eV (λ = 448 nm). (right) the extracted PL intensities showing a 50% reduction